SEQUENTIAL METHOD TO COMPUTE MULTIOBJECTIVE OPTIMAL LOW-THRUST EARTH ORBIT TRANSFERS

David Morante González[*], *Manuel Sanjurjo Rivo*[†], *and Manuel Soler Arnedo*[‡]

ABSTRACT

A sequential algorithm for optimizing low-thrust Earth orbit transfers in terms of the propellant consumed is proposed. The dynamical model includes the effect of the Earth shadow and the J_2 effect of the gravitational potential. The algorithm is based on two steps of growing complexity. In the first step, a near-optimal solution is obtained using simplified dynamics. In the second step, a hybrid approach embedded in a direct collocation scheme is used to consider the optimal coast arcs out of the Earth shadow. This novel approach is a continuation of a previous work in which the minimum time problem was solved. The ultimate goal of the work is to develop a robust and flexible tool that addresses the multi-objective design of low thrust transfers in Earth orbit. Hence, the user will not only obtain just point solutions, but will be able to explore the set of Pareto optimal trajectories for these two objectives.

Index Terms— Low-thrust, Hybrid Optimal Control, Multiobjective

1. INTRODUCTION

Low-Thrust propulsion is currently considered by all space actors as a key and revolutionary technology for the new generations of commercial and scientific satellites. Its major attraction lies on the reduction of propellant mass [1] due to its high specific impulse when compared with chemical propulsion. Different electric propulsion (EP) technologies have been proposed for orbit transfer and station keeping improving the performance of the current Earth satellites with an all-electrical platform [2]. Among the EP technologies, Hall Effect Thrusters (HETs), Ion Thrusters (ITs) and Arcjets have been already considered as possible candidates for the Earth-orbit transfer [3, 4, 5]. In fact, the performance of low-thrust solar EP for deep space scenarios has been tested in actual missions such as NASA Deep Space 1 [6] and ESA SMART-1 [7] or even in the most recent Dawn mission to Ceres [8]. Additionally, in 2015 Boeing launched its 702SP platform, which has been the first satellite in implementing all-electric propulsion for orbit raising and station keeping, saving thousands of kilograms of mass and decreasing the satellite price and its launch by hundreds of millions of dollars [9].

The design of low-thrust trajectories in such scenarios can be formulated as a Hybrid Optimal Control Problem. However, finding the control profile and the unknown switching sequence of coasting/thrust modes that satisfy the mission's constraints and minimize a certain cost is still a challenging open problem for several reasons. Although technology dependent, thrust acceleration is usually much lower than the gravitational acceleration, and, as a consequence, transfer times are usually several months for a typical trajectory from Geostationary Transfer Orbit orbit (GTO) to Geostationary Earth Orbit (GEO). In addition to this, due to the long time of flight, perturbing forces of the two-body-problem have an amplified impact in low-thrust trajectories when compared to impulsive trajectories. Therefore, perturbations due to oblateness, aerodynamic drag, or third-body may be included in the model. Finally, when considering solar EP, the shadow of the Earth has a significant effect since no thrust is generated when the spacecraft passes through it. In short, both low-thrust and long transfer times together with the unknown burn/coast sequence translate into a very challenging computational problem.

Historically, the first approaches consisted of "ad hoc" analytical solutions to specific problems. In those works, either the control law or the trajectory (even both of them) are assumed to be known "a priori". In this line, the seminal works of Forbes [10], Tsien [11], Lawden [12], Edelbaum [13], deserve a special mention. After them and extending the study of different problems, solutions for particular trajectory shapes were developed, such as the logarithmic spiral by Tsu [14] or the more versatile exponential sinusoid presented by Petropoulos [15]. The dynamical description of the problem is usually given either by averaging techniques or by asymptotic analysis. The averaging method has been extensively used and has proved to be effective [16]. Also Y. Gao [17] applied the averaging method using a predefined control law considering Earth J_2 and shadow effects. On the other hand, asymptotic analysis, in particular multiple-scales asymptotic analysis, has also been an effective way to obtain analytical solutions for particular problems [18, 19, 20]. The short-

[*]PhD student, Bioengineering and Aerospace Engineering Department, Universidad Carlos III de Madrid, Avenida de la Universidad, 30, Leganés.

[†]Assistant Professor, Bioengineering and Aerospace Engineering Department, Universidad Carlos III de Madrid, Avenida de la Universidad, 30, Leganés.

[‡]Assistant Professor, Bioengineering and Aerospace Engineering Department, Universidad Carlos III de Madrid, Avenida de la Universidad, 30, Leganés

comings of the analytical approaches lie in the compulsory approximation of the dynamical model and the specificity of each method.

The optimal control problem is also tackled with classical direct and indirect methods [21] [22]. Within indirect methodologies, it is worth noting the approach by Haberkon et al. [23], which combines a shooting method with a homotopic formulation to obtain a suitable initial guess, circumventing thus one of the classical drawbacks of indirect methods, i.e., that of finding an initial guess to lagrange multipliers. Nonetheless, neither a high fidelity dynamical model, nor the eclipse effect were considered. On the other hand, a typical strategy to tackle more realistic dynamics and constraints is to use the so-called direct methods, which discretize the continuous optimal control problem to obtain a Nonlinear Programming problem (NLP). This approach has been explored since the 90s [24] and recently used by Betts [25], addressing the challenges of including eclipse constraint within a high-fidelity dynamical model in large duration transfers. In his work, he proposed a two level algorithm, in which the switching sequence is predetermined by a receding horizon algorithm, and then the optimal trajectory is obtain as the solution of a Multiphase Optimal Control Problem.

However, the previous techniques did not incorporate the switching required to model coast phases out of the Earth shadow. As a solution, this problem can be tackle as a Hybrid Optimal Control Problem. Several approaches have been developed such as the hybrid Maximum Principle [26] or the two stage algorithms [27]. An alternative approach is to relax the binary functions associated to the mode sequence to obtain a convexification or embedding of binary constraints [28]. This technique, which is the basis of our methodology, converts the problem into a classical Optimal Control Problem, that can be solved as a NLP. Nevertheless, a sufficiently good initial guess is demanded for a good convergence to the solution [29].

In this paper, a sequential, yet robust and flexible, algorithm to address the shortcomings above mentioned is proposed. The problem is formulated as a Hybrid Optimal Control Problem, that is solved via a embedding technique using the Hermite-Simpson direct collocation method. In a similar fashion than in [25], the number and sequence of shadow/sunlight phases are determined in a previous step. For that purpose, we obtain the near-optimal control law proposed by Y. Gao [17], which also provides a suitable initial estimation for the state and control variables, as well as a for the thrusting/no-thrusting modes during sunlight.

The main contribution of the paper is the application of the embedding technique to the design of minimum-fuel Earth-orbit transfers using low-thrust. It allows to include the coasting mechanism out of the Earth shadow in the solution, which play a key role in this kind of trajectories.

2. HYBRID OPTIMAL CONTROL PROBLEM

Spacecraft flight dynamics equipped with electric propulsion systems can be described by a switched dynamical system, that is, a dynamical system with multiple modes of operation. These modes denote the switch on/off of the engine due to the Earth-shadow effect or due to a control decision to reduce the propellant consumption. Each flight mode is characterized by a different set of differential equations and constraints. Our goal is to obtain a numerical solution to the resulting hybrid optimal control problem, casting the problem as a nonlinear optimization program (NLP) and employ *off-the-shelf* NLP solvers.

Our approach follows the same line as in [30] and can be summarized in the following steps. First, we introduce binary control functions for each mode to formulate the hybrid optimal control problem as a Mixed Integer Optimal Control Problem (MIOCP) [31]. Next, we relax the binary functions and include a penalty term on the relaxation, so that as the weight of the penalty term increases, the relaxed solution converges to a binary function. Finally, we apply a collocation discretization rule [32] to convert the continuous problem into an NLP. We use the so-called Hermite-Simpson direct collocation method [32].

2.1. General Formulation

Let us consider a switched system described by a set of differential equations

$$\dot{x}(t) = f_q(x(t), u(t)),\ q \in Q := \{1, 2, \ldots, n_q\}, \quad (1)$$

where $x(t) \in \mathbb{R}^{n_x}$ represents the continuous states and $f_q : \mathbb{R}^{n_x} \times \mathbb{R}^{n_u} \to \mathbb{R}^{n_x}$ represents the dynamics in mode q. The input $u(t)$ is in a compact set $U \subset \mathbb{R}^{n_u}$. For spacecraft flight, x denotes the dynamic states of the spacecraft e.g., position and velocity and u denotes the control variables, e.g., thrust direction angles.

A switching sequence σ is defined as the timed sequence of active dynamical systems, or modes, as follows:

$$\sigma = [(t_0, q_0), (t_1, q_1), \ldots, (t_N, q_N)],$$

where N represents the number of mode switches (considering also the final time as a switch), and $q_i \in Q$ for $i = 0, 1, \ldots, N$. t_0 is the initial time, t_i for $i = 1, \ldots, N$, with $t_0 \leq t_1 \leq \cdots \leq t_N \leq t_{N+1}$ are the switching times. We define $t_f = t_{N+1}$ as the final time. The pair (t_i, q_i) for $1 \leq i \leq N$ indicates that at time t_i the dynamics change from mode q_{i-1} to q_i. Thus, in the time interval $[t_i, t_{i+1})$, referred to as the i-th phase/operation, the state evolution is governed by the vector field f_{q_i}. As an illustration, a spacecraft might be flying coasting and then switch at t_1 to a thrusting mode.

The state and control variables must fulfill constraints for each mode $q \in Q$, compactly represented as

$$h_q(x(t), u(t)) \leq 0, \quad (2)$$

where in the above $h_q : \mathbb{R}^{n_x} \times \mathbb{R}^{n_u} \to \mathbb{R}^{n_h}$. These constraints are used to capture limiting values, e.g. the maximum thrust available.

The objective in trajectory planning based on optimization is to find a feasible transfer trajectory that minimizes a desired cost function such as fuel or time of flight. The hybrid optimal control problem is thus as follows: given an initial condition $x(t_0)$, find a switching sequence σ and an input $u : [t_0, t_f] \to U$, that fulfill the dynamics (1), the constraints (2) and minimize a cost function $J(\sigma, u)$. That is, solve the following hybrid optimal control problem:

$$\begin{aligned} \min_{u,\sigma} \quad & J(u,\sigma) := \phi(x(t_f)) + \textstyle\sum_{i=0}^{N} \int_{t_i}^{t_{i+1}} L_{q_i}(x(t), u(t))dt \\ \text{s.t.} \quad & x(t_0) = x_0, \text{ and for } i \in [t_i, t_{i+1}],\ i = 0, \ldots, N, \\ & \dot{x}(t) = f_{q_i}(x(t), u(t)), \\ & h_{q_i}(x(t), u(t)) \leq 0. \end{aligned} \tag{3}$$

In the above, ϕ is referred to as the Mayer term, denoting a final cost, and the integral term in J is referred to as the Lagrange term, denoting a running cost. The final cost can be used to quantify the deviation from a desired final state, such as reaching a target orbit or a destination at a given time. The running cost can denote costs accumulated during the transfer orbit such as fuel consumption. The initial time t_0 is given while the final time t_f can be an optimization variable.

The hybrid optimal control problem defined above is challenging for several reasons. First, the unknown number of mode switches, switching sequence and switching times result in a non-classical Hybrid Optimal Control Problem. Second, the spacecraft is subjected to small perturbations during long transfer times. As a consequence, the dynamics and constraints are very non-linear.

2.2. Solution Approach

By adding new binary control variables, constraints and cost function, the Hybrid Optimal Control can be transformed to a Mixed Integer Optimal Control Problem. If the binary constraints are relaxed through a penalty term, it can be formulated as a classical optimal control problem as follows.

Let $w_q : [t_0, t_f] \to \{0, 1\}$ denote a binary control function for each mode $q = 1, \ldots, n_q$. Let $\bar{f} : \mathbb{R}^{n_x} \times \mathbb{R}^{n_u} \times \{0,1\}^{n_q}$ be defined as $\bar{f} = \sum_{q=1}^{n_q} w_q f_q$. By adding the constraint $\sum_{q=1}^{n_q} w_q(t) = 1$, we ensure there is one active mode at each time t and so the dynamical system is well-defined. Similarly, define $\bar{h} = \sum_{q=1}^{n_q} w_q h_q$ and $\bar{L} = \sum_{q=1}^{n_q} w_q L_q$.

Now, let us relax $w_q(t)$ by allowing it to belong to $[0, 1]$ instead of $\{0, 1\}$. Then, we define $\beta_q : [t_0, t_f] \to [0, 1]$ for $q = 1, \ldots, n_q$, as a vector of auxiliary optimization variables, with $\beta_q(t) = w_q(t)(w_q(t) - 1)$. We define a penalty cost function $l : [0, 1] \to \mathbb{R}_{\geq 0}$, where l is strictly monotonically decreasing and $l(1) = 0$. With the relaxation and the penalty term, we formulate a classical optimal control problem as:

$$\begin{aligned} \min_{u,w,\beta} \quad & J(u,w,\beta) = \phi(x(t_f)) \\ & + \textstyle\int_{t_0}^{t_f} \left(\bar{L}(x(t), u(t), w(t)) + \alpha \sum_{q=1}^{n_q} l(|\beta_q(t)|) \right) dt \\ \text{s.t.} \quad & x(t_0) = x_0, \text{and } \forall t \in [0, t_f] \\ & \dot{x}(t) = \bar{f}(x(t), u(t), w(t)), \\ & \bar{h}(x(t), u(t), w(t)) \leq 0, \\ & \beta_q(t) \in [0, 1],\ q = 1, \ldots, n_q, \\ & \beta_q(t) = w_q(t)(w_q(t) - 1),\ q = 1, \ldots, n_q \\ & \textstyle\sum_{q=1}^{n_q} w_q(t) = 1. \end{aligned} \tag{4}$$

The control variables in the transformed problem are the input $u(t)$, the auxiliary inputs $\beta_q(t)$, the switching law $w_q(t)$ for $t \in [t_0, t_f]$, $q \in Q$ and the final time t_f. The constant α is a design parameter. While integer constraints are not explicitly added, the penalty term ensures that in practice for sufficiently large α, the optimized solution would approach $|\beta_q(t)| = 0$ and consequently, $w_q(t) \in \{0, 1\}$ for each $q \in Q$.

3. DYNAMICAL MODEL

The motion of a spacecraft of negligible mass in orbit around a central body can be described by a system of second-order ordinary differential equations:

$$\ddot{\boldsymbol{r}} + \mu \frac{\boldsymbol{r}}{r^3} = \boldsymbol{a}_d \tag{5}$$

where the radius $r = ||\boldsymbol{r}||$ is the magnitude of the inertial position vector $\boldsymbol{r}$, μ is the standard gravitational parameter of the central body and $\boldsymbol{a}_d$ is defined as the disturbing acceleration. The differential equation (5) is usually formulated using the classical set of orbital elements $(a, e, i, \Omega, \omega, M)$ to define the state vector. However, these elements exhibit singularities for $e = 0$, and $i = 0\,^\circ, 90\,^\circ$, which are both cases of interest for trajectories arriving to or departing from geostationary orbits. In order to avoid this singularities, Betts [25] uses a set of modified equinoctial elements as presented by Walker [33]. Following them, the dynamical system can be described in terms of the state variables

$$\tilde{\boldsymbol{x}} = [p, f, g, h, k, L] \tag{6}$$

the control variables

$$\boldsymbol{u} = [u_1, u_2, \omega] \tag{7}$$

and the parameters $\boldsymbol{p}$ resulting in

$$\dot{\tilde{\boldsymbol{x}}} = \boldsymbol{A}(\tilde{\boldsymbol{x}})\boldsymbol{a}_d + \boldsymbol{b} = \tilde{\boldsymbol{f}}(\tilde{\boldsymbol{x}}, \boldsymbol{u}, \boldsymbol{p}, t) \tag{8}$$

The equinoctial dynamics are defined by the matrix

$$\boldsymbol{A} = \begin{bmatrix} 0 & \frac{2p}{q}\sqrt{\frac{p}{\mu}} & 0 \\ \sqrt{\frac{p}{\mu}}\sin L & \sqrt{\frac{p}{\mu}}\frac{1}{q}\{(q+1)\cos L + f\} & -\sqrt{\frac{p}{\mu}}\frac{g}{q}\{h\sin L - k\cos L\} \\ -\sqrt{\frac{p}{\mu}}\cos L & \sqrt{\frac{p}{\mu}}\frac{1}{q}\{(q+1)\sin L + g\} & \sqrt{\frac{p}{\mu}}\frac{f}{q}\{h\sin L - k\cos L\} \\ 0 & 0 & \sqrt{\frac{p}{\mu}}\frac{s^2\cos L}{2q} \\ 0 & 0 & \sqrt{\frac{p}{\mu}}\frac{s^2\sin L}{2q} \\ 0 & 0 & \sqrt{\frac{p}{\mu}}\frac{1}{q}\{h\sin L - k\cos L\} \end{bmatrix}$$

and the vector

$$\boldsymbol{b}^T = \begin{bmatrix} 0 & 0 & 0 & 0 & 0 & \sqrt{\mu p}\left(\frac{q}{p}\right)^2 \end{bmatrix} \tag{9}$$

where

$$q = 1 + f\cos L + g\sin L \tag{10}$$

$$s^2 = 1 + h^2 + k^2 \tag{11}$$

Equation (8) can be better expressed considering the True Longitude L as the independent variable, instead of the physical time t, given that low-thrust transfer are characterized by very long times [34]. Physically this represents an angle in the orbit plane and consequently one complete orbit revolution corresponds to a change of 2π in the variable L.

Thus, the new equation of motion can be expressed as a function of the system in (8)

$$\boldsymbol{f}(\mathbf{x}, \boldsymbol{u}, \boldsymbol{p}, L) = \tilde{\boldsymbol{f}}(\tilde{\boldsymbol{x}}, \boldsymbol{u}, \boldsymbol{p}, t)/\tau \tag{12}$$

$$\tau = \tilde{\boldsymbol{f}}_6(\tilde{\boldsymbol{x}}, \boldsymbol{u}, \boldsymbol{p}, t) \tag{13}$$

with the new set of dependent variables

$$\boldsymbol{x} = [p, f, g, h, k, t] \tag{14}$$

3.1. Perturbing and Thrust accelerations

The disturbing acceleration $\boldsymbol{a}_d$ can be expressed as

$$\boldsymbol{a}_d = \boldsymbol{a}_g + \boldsymbol{a}_{3b} + \boldsymbol{a}_T \tag{15}$$

with contributions due to oblate Earth effects $\boldsymbol{a}_g$, secondary bodies $\boldsymbol{a}_{3b}$, and thrust $\boldsymbol{a}_T$. A more detailed description of these perturbations is given in [34].

3.1.1. Thrust acceleration

The thrust steering law is completely determined by the time varying angles u_1 and u_2. Here u_1, is the thrust pitch angle measured in the orbital plane off the circumferential direction, positive away from the center of mass, and u_2 is the thrust angle measured off the orbital plane and perpendicular to it, positive in the direction of the angular momentum vector. With this formulation, the thrust acceleration can be expressed projected in the Radial Reference Frame $(\hat{\mathbf{i}}, \hat{\mathbf{j}}, \hat{\mathbf{k}})$

$$\mathbf{a}_T = a_T\omega[\cos u_2 \sin u_2\hat{\mathbf{i}} + \cos u_2 \cos u_1\hat{\mathbf{j}} + \sin u_2\hat{\mathbf{k}}] \tag{16}$$

where the unit vectors are

$$\hat{\mathbf{i}} = \frac{\boldsymbol{r}}{r}, \qquad \hat{\mathbf{k}} = \frac{\boldsymbol{r}\times\boldsymbol{v}}{||\boldsymbol{r}\times\boldsymbol{v}||}, \qquad \hat{\mathbf{j}} = \hat{\mathbf{k}}\times\hat{\mathbf{i}} \tag{17}$$

Also, ω is a binary variable with two possible values $\{0, 1\}$. It controls the spacecraft modes. When $\omega = 0$, engines are off, whereas $\omega = 1$ means that spacecraft is in burn phase. The parameter a_T measures the magnitude of the acceleration that the thruster can provide. It is a function of the input power P, the thruster efficiency η, its specific impulse I_{sp}, the Earth gravitational acceleration at sea level g_0 and the spacecraft mass m.

$$a_T = \frac{2\eta P}{m g_0 I_{sp}} \tag{18}$$

Note that, the mass flow rate $\dot{m}$ is constant and can be expressed as

$$\dot{m} = -\frac{2\eta P}{(g_0 I_{sp})^2} \tag{19}$$

To reduce the wrapping in the control due to the periodicity of the angular variables, we restrict the angles to

$$-\pi \le u_1 \le \pi \tag{20}$$

$$-\pi/2 \le u_2 \le \pi/2 \tag{21}$$

Other alternatives to define the control are possible [25], such as the thrust-unitary-vector projections onto the Radial Orbital frame, but this formulation increases the size of the problem, as it incorporates one additional variable and a path constraint.

3.2. Eclipse Contraints

To accurately model the solar electric propulsion system it is necessary to model the trajectory as it passes through the shadow of the Earth, because no thrust is generated $(a_T = 0)$. The location of the eclipse is a function of $\boldsymbol{s}_s$ which is the vector from the Earth to the sun, with norm $s_s = ||\boldsymbol{s}_s||$. Let us define the solar unit vector $\hat{\boldsymbol{s}}$ as

$$\hat{\boldsymbol{s}} = \frac{\boldsymbol{s}_s}{s_s} \tag{22}$$

and the projected spacecraft position that is given by

$$\bar{\boldsymbol{r}} = (\boldsymbol{r}^T\hat{\boldsymbol{s}})\hat{\boldsymbol{s}} \tag{23}$$

and the auxiliary vector

$$\boldsymbol{\delta} = \boldsymbol{r} - \bar{\boldsymbol{r}} \tag{24}$$

Under the cylindrical shadow model [35], the eclipse constraint can be computed according to the following rules:

Rule 1: A shadow terminator can only be encountered if $\boldsymbol{r}^T \hat{\boldsymbol{s}} < 0$ and $||\boldsymbol{\delta}|| = R_e$

Rule 2: The spacecraft will be in sunlight if $||\boldsymbol{\delta}|| > R_e$

Rule 3: The spacecraft will be in shadow if $||\boldsymbol{\delta}|| < R_e$

4. SEQUENTIAL OPTIMIZATION ALGORITHM

The proposed approach can be used to solve both, minimum-time and minimum-fuel problems. However, the phase structure for each problem is different. In the former, the simplification $w = 1$, can be done, as the thrust will be always applied out of the Earth shadow. Thus, a simplified phase structure as in Fig. 1 can is assumed . In the former, w can take different values between, resulting in a more complicated phase structure as it can be seen in Fig. 2. A detailed description on how to solve the minimum-time problem was done in [36]. Thus, we will focus on the minimum-fuel problem hereafter, being the objective function

$$J = \int_{t_0}^{t_f} \dot{m} dt + \alpha \sum_{q=1}^{n_q} l(|\beta_q(t)|) \, \big) dt \tag{25}$$

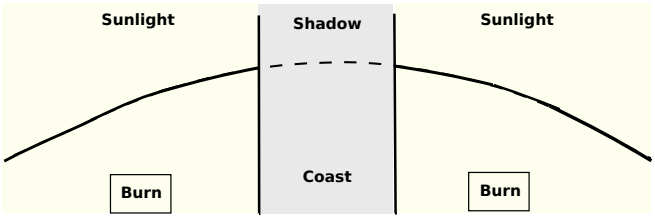

Fig. 1. Burn/coast arcs in the minimum-time problem

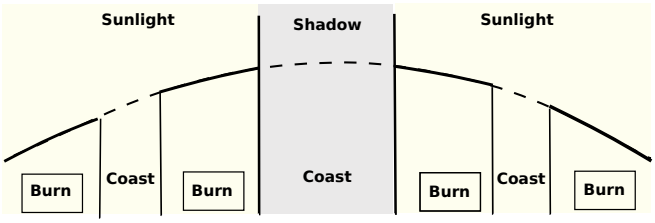

Fig. 2. Burn/coast arcs in the minimum-fuel problem

4.1. Initial guess generation

From this step we obtain the number and sequence of shadow/ sunlight phases as well as a sufficiently good initial estimate of the control and state variables. The method applied relies on the work of Y. Gao [17], who defined three control laws that are only applied over an arc within each orbital revolution. Within this model, the effect of propellant consumption, the constraint of non-thrusting along the Earth-shadow, the Earth-oblateness effect due to J_2 and the discontinuous thrusting during sunlight are included. As a result, he obtained an analytical expression for the Gauss's variational equations averaged over an orbital revolution. In this way, the trajectory propagation time is greatly reduced while satisfactory solution accuracy is maintained.

The main reason to use this method lies on its capability of including discontinuous thrusting out of the Earth shadow.

4.2. Control and State Discretization

Let us define the switching sequence σ as the sequence of shadow/sunlight modes as a function of the true Longitude L.

$$\sigma = [(L_{0,1}, q_0), ..., (L_{k,1}, q_k), ..., (L_{N,1}, q_N)] \tag{26}$$

where N is he known number of phases and q_k are the known modes of operations, i.e. q_k = *shadow* for $k = 1, 3, 5, ..., N$, and q_k = *sunlight* for $k = 2, 4, 6, ...N$.

Let us define the discrete state $x_{k,i}$ and control $u_{k,i}$ for $i = 1, ..., n_k$, where n_k is the number of grid points within each phase k. Note that, the burn/coast phases during sunlight are determined by the relax binary variable $w_{k,i}$, which is only defined for $k = 2, 4, 6, ..., N$.

Let us define the node spacing $\Delta\phi_k$ as the angular distance between two adjacent nodes

$$\Delta\phi_k = \frac{L_{k+1,1} - L_{k,1}}{n_k} \tag{27}$$

An initial estimation for $L_{k,1}$ and $L_{k+1,1}$ is known before defining the grid, as they correspond to the shadow entrance and exit locations. Using this information, we can define a grid in which the node spacing $\Delta\phi_k$ is proportional to the arc length. Thus, the number of nodes for each phase can be computed as:

$$n_k = \frac{L_{k+1,1} - L_{k,1}}{2\pi} \left| \frac{||\bar{r_k}|| - ||\bar{r}||}{||\bar{r}||} \right| \mathcal{N} \tag{28}$$

where $\bar{r_k}$ is the mean value of r during phase k and $\bar{r}$ is the mean value of r during the whole trajectory.

$\mathcal{N}$ is a user-defined parameter that means the number of nodes in a phase that covers a complete revolution in which $\bar{r_k} = \bar{r}$ is satisfied.

In the following section, results are presented as a function of the mean node spacing

$$\bar{\Delta\phi} = \frac{\sum_{k=1}^{N} \Delta\phi_k}{N}$$

which is consider as a representative value of the fineness of the grid.

5. NUMERICAL RESULTS

In this section a test case scenario is defined to illustrate the performances and stability of the method proposed. The minimum-fuel transfer trajectory from a geostationary transfer orbit (GTO) to a geostationary equatorial orbit (GEO) is considered. The classical orbital elements of the departure and arrival orbits are presented in Table 1. Also the spacecraft characteristics, such as the input power P, thruster efficiency η, specific impulse I_{sp}, and they initial spacecraft mass m_0 are summarized in Table 2. Note that the engine parameters correspond to those of a Ion Thruster (IT), because a Hall thruster is characterized by a lower I_{sp} and a higher thrust.

Table 1. Departure and Arrival Orbits Parameters

Orbits	a/R_e	e	i (deg)	Ω (deg)	ω (deg)
GTO	3.820	0.731	27	99	0
GEO	6.6107	10^{-4}	10^{-4}	–	–

Table 2. Spacecraft Parameters

P (kW)	$I_{sp}(s)$	η	m_0 (kg)	$T/(m_0 g_0)$
5	3300	0.65	450	$4.55 \cdot 10^{-5}$

The initial date is set for 1 January 2008 for all the simulations, which are performed using a Intel Core i7 (2,5GHz). Also, the resulting large scale NLP have been solved using the Interior-point method IPOPT [37]. Note that all the solutions presented in this section have to be regarded as local optimal solutions, as no global search is done.

5.1. Pareto Front

Several minimum-fuel optimal control problem are solved for different fixed time of flights. Propellant masses and transfer times for all the cases are presented in Table 3 and in Fig. 3, where it is indicated that the fuel consumption decrease with the increasing of the transfer times. However, the propellant masses decreasing rates become smaller as the transfer times become longer, e.g. increasing transfer times from 75 to 100 days save about 22.5% of propellant mass, whereas and increment from 100 to 200 days saves only 4%.

Table 3. Propellant masses vs transfer times

Transfer Time $(days)$					
66.7	75	100	120	150	200
Propellant mass (Kg)					
36.50	31.27	28.29	27.58	27.27	27.13

Note that two limiting values can be highlighted in Fig. 3. On the one hand, no feasible solutions exist for shorter transfer times than 66.7 days, which corresponds to the minimum-time solution, which means continuos thrusting during sunlight.

On the other hand, there is a minimum propellant mass required for the transfer. As the time of flight increases, the duration of the burn arcs is reduced. When transfer times are considerably long, the duration of the burn arcs will be negligible and the less possible propellant will be consumed. Thus, this transfer can be modeled as an impulsive maneuver but considering the I_{sp} of the IT. This maneuver consists on the combined maneuver to change velocity and the orbit plane in one impulse. The required ΔV can be obtained as

$$\Delta V = \sqrt{V_A^2 + V_F^2 - 2V_A V_s \cos(\Delta i)} \tag{29}$$

where V_A is the velocity in the Apogee of the GTO, V_F the velocity in GEO and Δi refers to the required inclination change. Given the rocket equation

$$m_{f,min} = m_0 e^{-\Delta V/(g_0 I_{sp})} \tag{30}$$

the fuel consumption $m_{f,min}$

$$m_{f,min} = 24.4kg \tag{31}$$

The time histories of the classical orbital elements, i.e. the semimajor-axis, eccentricity and inclination for 75, 100, 120, 150 days are plotted in Figs. 4,5 and 6 respectively. Additionally, the 3 dimensional trajectory for 150 days is shown in Fig. 8, where blue, red and black arcs correspond to burn, coast and shadow arcs respectively. Note the importance of taking coast into account, as it covers most of the trajectory.

5.2. Performance analysis

The algorithm should be robust and efficient. Robust means that it should be numerically stable. Efficient means that the algorithm should render accurate results with low time-consumption. For the sake of brevity, only the results for 150 days will be shown.

On the one hand, numerical stability for Direct Transcription or Collocation Methods for solving Optimal Control Problems, implies that the discrete solution should approach the continuos one, as the grid becomes finer. In other words,

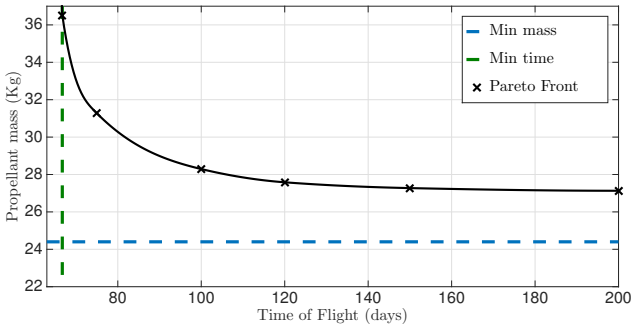

Fig. 3. Pareto front for the GTO-GEO transfer

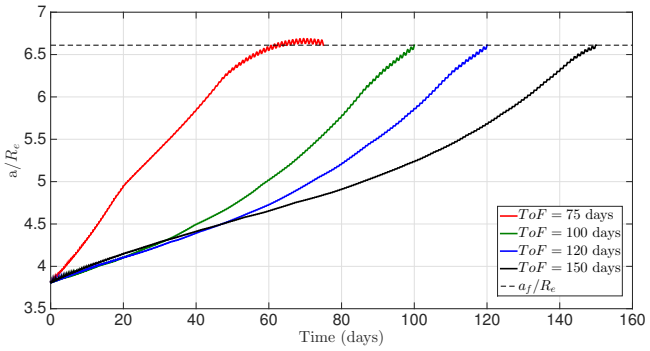

Fig. 4. Time histories of the semimajor-axis for GTO-GEO transfers

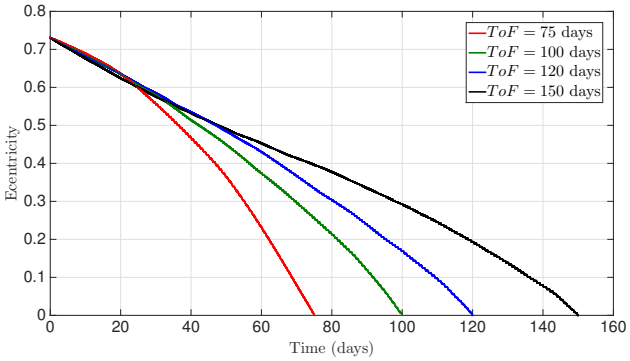

Fig. 5. Time histories of the eccentricity for GTO-GEO transfers

stability ensures that the problem is well-posed. As a consequence, a deep analysis of the solution is performed for different grid sizes, i.e. for different $\Delta\bar{\phi}$.

The computational performance of the optimization algorithm for 9 different grid sizes are shown in Table 4. The number of variables and constraints illustrates the size of the problem. In Fig. 7 it can be seen that, as the grid becomes

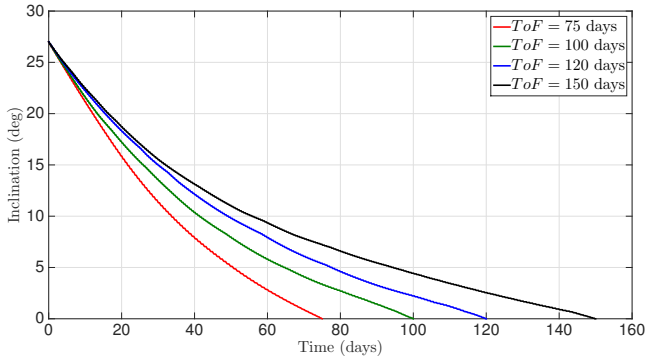

Fig. 6. Time histories of inclination for GTO-GEO transfers

finer, the better the objective value but the higher the computational cost, as the size of the problem increases. As an illustration, to obtain a reduction of 0.94% in the objective, the number of variables is increased by 7 and the computational time is 20 times higher.

The parameter $Obj_{\%,k}$ shown in Fig. 7 measures the difference between the objective and best objective obtained.

$$Obj_{\%,k} = 100\frac{Obj_{k=9} - Obj_k}{Obj_{k=9}} \quad \text{for} \quad k = 1...9 \qquad (32)$$

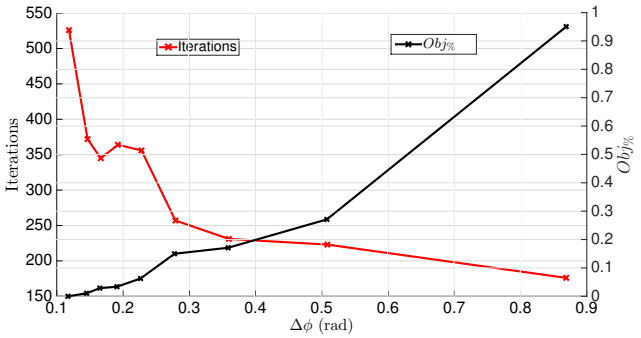

Fig. 7. Performances of the Algorithm for 150 days

5.3. Stability Analysis

Whereas we have completely determined the switch-on/off instants at shadow terminators, which are provided by the optimal solutions for $L_{k,1}$, it is not for the switch-on/off instants during sunlight, due to the discretization scheme. As an example, let suppose that $w_{k,2} = 0$ and $w_{k,3} = 1$ as it is illustrated in Fig. 10(a). Thus, the optimal switching could be located at any location within the interval $[L_{k,2}\ ,L_{k,3}]$, whose amplitude is equal to $\Delta\phi_k$. In Figure **??** it can be appreciated the accuracy in the determination of the control law as a function of the grid sizes used in this example.

Table 4. Performances of the Algorithm for 150 days

k	$\Delta\phi(rad)$	Obj.(kg)	Iter.	Variables	Constraints	CPU time(s)	ε_{min}	ε_{max}	ε_{3body}
1	0,8690	27,4910	176	19829	15971	188,03	0,1584	0,6028	0,6131
2	0,5085	27,3059	223	33885	26730	413,27	0,0710	0,3244	0,3359
3	0,3599	27,2787	231	47873	37445	601,58	0,0525	0,2211	0,2323
4	0,2792	27,2729	257	61928	48212	875,37	0.0409	0,1708	0,1821
5	0,2280	27,2492	346	75919	58924	1442,36	0,0316	0,1285	0,1549
6	0,1924	27.2414	364	89900	69632	1798,44	0,0311	0,1003	0,1282
7	0,1665	27,2399	345	103860	80319	1974,34	0,0268	0,0857	0,1127
8	0,1466	27,2350	372	117972	91134	2384,36	0,0241	0,0857	0,0992
9	0,1185	27,2322	526	145956	112563	4276,58	0,0201	0,0704	0,0824

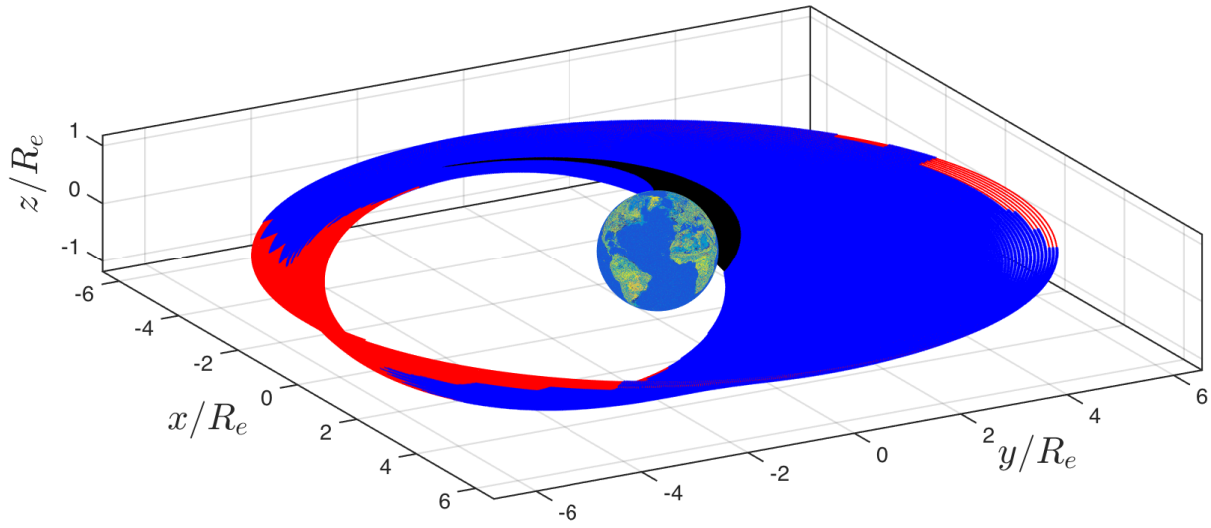

Fig. 8. GTO-GEO transfer trajectory for 150 days

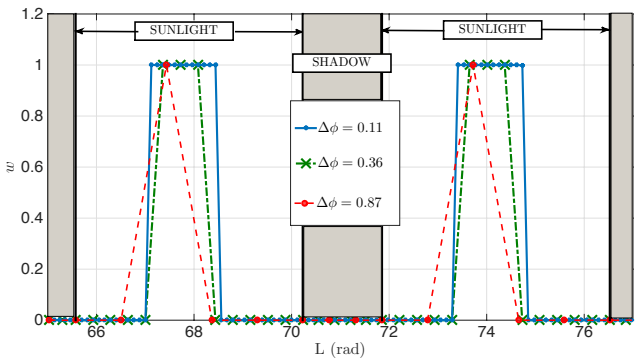

Fig. 9. Control modes as a function of the node spacing

Our goal is to measure the effect of this indetermination and thus to prove the suitability and applicability of the optimal control law proposed. Thus, we use the precise numerical integration, in particular a Runge-Kutta 7(8), to simulate the transfer trajectories following the obtained control law. We characterize this suitability by a minimum and a maximum error , which are ε_{min} and ε_{max} respectively. The error is defined as the difference between the integrated final conditions and the target ones in terms of the classical orbital elements.

$$\varepsilon = \left|\frac{a(t_f) - a^*(t_f)}{a^*(t_f)}\right| + \left|e(t_f) - e^*(t_f)\right| + \left|i(t_f) - i^*(t_f)\right| \tag{33}$$

The minimum values of the error are found when the switch is performed at the midpoint of the interval (Fig. 10(b)), whereas the maximum one is located when the switching instants are located at the edges of the interval (Fig. 10(c) and Fig. 10(d)). As it is expected, the finer the grid is, the lower the error, as well as the difference between the maximum and the minimum (Fig.11). However, a finer grid implies a larger size of the problem and thus a higher computational cost.

In addition, a propagation considering 3^{rd} perturbations is

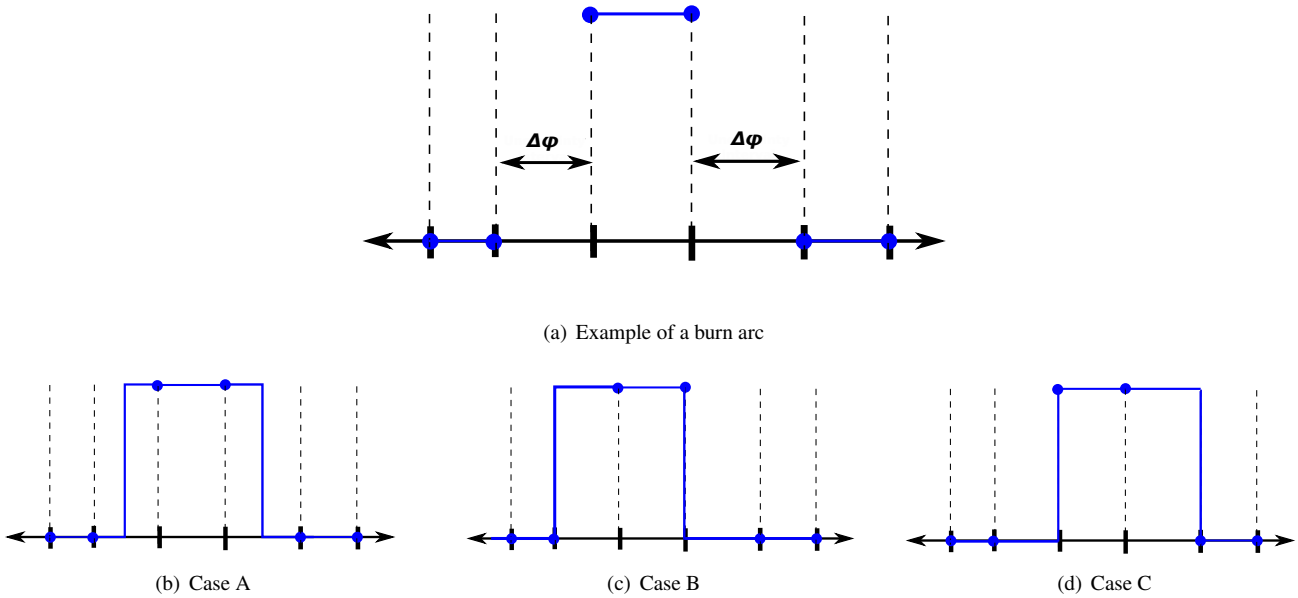

(a) Example of a burn arc

(b) Case A

(c) Case B

(d) Case C

Fig. 10. Definition of the switching instants

done, including both, the moon and sun influence. As a result, we obtain that the deviations ε_{3body}that we obtain from the discretization of the control, are of the order of those obtain when they are not included. Thus, is reasonable not to include these perturbation in our model. However the same analysis should be carried out considering other perturbations.

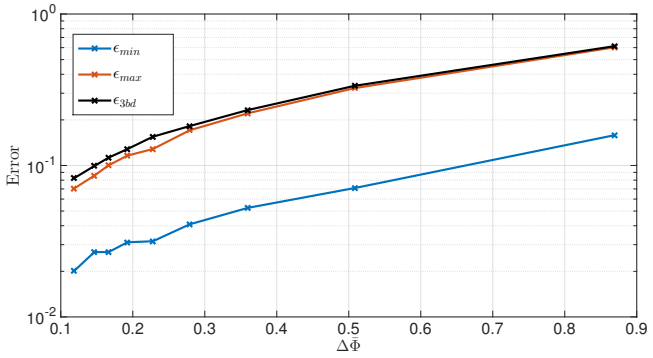

Fig. 11. Deviations from the targeting conditions

6. SUMMARY AND CONCLUSIONS

A sequential scheme have been presented for constructing optimal low-thrust orbit transfer that addresses the impact of eclipse regions, including also the coasting mechanism during sunlight. The approach is illustrated by computing different minimum-fuel transfers to a Geosynchronous orbit for different Time of flights, obtaining the set of solutions that define the Pareto Front. Moreover, the stability of the algorithm is assed by testing each case for different grid sizes.

The precise numerical integration is used to simulate the transfer trajectories following the obtained control law, using both, the same dynamical model and including third-body perturbations. The results obtained by the Nonlinear Programming solver and by the integration differs from each other, as a result of the control discretization. In order to increase the matching between the solutions, a finer grid should be used. In addition, the error could be minimize by setting the switching instants between modes at the midpoint of the interval between the nodes where they are defined.

Future work will explore its application to a more complex scenario such as a LEO-GEO case.We will also analyze the suitability of the method including a dynamical model of higher fidelity.

The ultimate goal of this tool is to enhance flexibility according to detail-level requirements, to improve robustness and to head for automation in optimizing low-thrust transfer trajectories.

7. ACKNOWLEDGEMENTS

This work has been partially supported by Spanish Government through grant TRA2014-58413-C2-2-R. The project has been funded under RD&I actions of Programa Estatal de Investigación, Desarrollo e Innovación Orientada a los Retos de la Sociedad (call 2014).

8. REFERENCES

[1] *URSI White Paper on Solar Power Satellite (SPS) Systems and Report of the URSI Inter-Commission Working Group on SPS*, Number 321. Radio Science Bulletin, June 2007.

[2] Atri Dutta, Paola Libraro, N Jeremy Kasdin, Edgar Choueiri, and Philippe Francken, "Design of next generation all-electric telecommunication satellites," in *AIAA International Communication Satellite Systems Conference, Florence, Italy*, 2013.

[3] M Martinez-Sanchez and James E Pollard, "Spacecraft electric propulsion-an overview," *Journal of Propulsion and Power*, vol. 14, no. 5, pp. 688–699, 1998.

[4] FS Gulczinski and Ronald A Spores, "Analysis of hall-effect thrusters and ion engines for orbit transfer missions," *AIAA Paper*, vol. 96, 1996.

[5] Mitat A Birkan, "Arcjets and arc heaters-an overview of research status and needs," *Journal of Propulsion and Power*, vol. 12, no. 6, pp. 1011–1017, 1996.

[6] M. D. Rayman, P. Varghese, D. H. Lehman, and L. L. Livesay, "Acta astronautica," *Results from the Deep Space 1 Technology Validation Mission*, vol. 47, pp. 475–487, 2000.

[7] G. Racca, A. Marini, L. Stagnaro, and et al., "Smart-1 mission description and development status," *Planetary and Space Science*, vol. 50, pp. 1323–1337, 2002.

[8] M. D. Rayman, T. C. Frashetti, C. A. Raymond, and C. T. Russel, "Dawn: A mission in development for exploration of main belt asteroids vesta and ceres," *Acta Astronautica*, vol. 58, pp. 605–616, 2006.

[9] Steven A. Feuerborn, Julie Perkins, and David A. Neary, "Finding a way: Boeing's all electric propulsion satellite," in *49th AIAA/ASME/SAE/ASEE Joint Propulsion Conference. July*, 2013.

[10] G. F. Forbes, "The trajectory of a powered rocket in space," *Journal of the British Interplanetary Society*, vol. 9, pp. 75–79, 1950.

[11] H.S. Tsien, "Take-off from satellite orbit," *Journal of the American Rocket Society*, vol. 23, pp. 233–236, 1953.

[12] D.F. Lawden, "Optimal intermediate-thrust arcs in gravitational field," *Acta Astronautica*, vol. 8, pp. 106–123, 1962.

[13] Theodore N. Edelbaum, "Optimal low-thrust rendezvous and station keeping," *AIAA Journal*, vol. Vol. 2, No. 7, pp. 1196–1201, 1964.

[14] T. C. Tsu, "Interplanetary travel by solar sail," *Journal of the American Rocket Society*, vol. 29, pp. 422–427, 1959.

[15] A. Petropoulos and J. Longuski, "Shape-Based Algorithm for the Automated Design of Low-Thrust, Gravity Assist Trajectories," *Journal of Spacecraft and Rockets*, vol. 41, pp. 787–796, Sept. 2004.

[16] A. E. Petropoulos, "Some analytic integrals of the averaged variational equations for a thrusting spacecraft," *The Interplanetary Network Progress Report*, vol. 42-150, 2002.

[17] Yang Gao, "Near-optimal very low-thrust earth-orbit transfers and guidance schemes," *Journal of guidance, control, and dynamics*, vol. 30, no. 2, March–April 2007.

[18] A. H. Nayfeh, *Perturbation Methods*, John Wiley & Sons, Inc., 1973.

[19] J. Kevorkian and J. Cole, *Perturbation methods in applied mathematics*, Springer-Verlag, 1981.

[20] Juan Luis Gonzalo and Claudio Bombardelli, "Asymptotic solution for the two body problem with radial perturbing acceleration," in *Advances in the Astronautical Sciences*, Santa Fe, New Mexico, USA, January 26-30 2014, AAS/AIAA, number AAS 14-226.

[21] John T Betts, "Survey of numerical methods for trajectory optimization," *Journal of guidance, control, and dynamics*, vol. 21, no. 2, pp. 193–207, 1998.

[22] Anil V Rao, "A survey of numerical methods for optimal control," *Advances in the Astronautical Sciences*, vol. 135, no. 1, pp. 497–528, 2009.

[23] Thomas Haberkorn, Pierre Martinon, and Joseph Gergaud, "Low thrust minimum-fuel orbital transfer: a homotopic approach," *Journal of Guidance, Control, and Dynamics*, vol. 27, no. 6, pp. 1046–1060, 2004.

[24] C. A. Kluever and S. R. Oleson, "Direct Approach for Computing Near-Optimal Low-Thrust Earth-Orbit Transfers," *Journal of Spacecraft and Rockets*, vol. 35, pp. 509–515, July 1998.

[25] John T. Betts, "Very low-thrust trajectory optimization using a direct sqp method very low-thrust trajectory optimization using a direct sqp method," *Journal of Computational and Applied Mathematics*, vol. 120, pp. 27–40, 2000.

[26] H.J. Sussmann, "A maximum principle for hybrid optimal control problems," in *IEEE Conference on Decision and Control*, 1999, vol. 1, pp. 425–430.

[27] Xuping Xu and Panos Antsaklis, "Results and perspectives on computational methods for optimal control of switched systems," in *Hybrid Systems: Computation and Control*, Oded Maler and Amir Pnueli, Eds., vol. 2623 of *Lecture Notes in Computer Science*, pp. 540–555. Springer, 2003.

[28] Richard Meyer, Miloš Žefran, and Raymond A DeCarlo, "A comparison of the embedding method to multi-parametric programming, mixed-integer programming, gradient-descent, and hybrid minimum principle based methods," *arXiv preprint arXiv:1203.3341*, 2012.

[29] Bruce A. Conway, *Spacecraft Trajectory Optimization*, Cambridge, 2010.

[30] M. Soler, M. Kamgarpour, J. Lloret, and J. Lygeros, "A hybrid optimal control approach to fuel-efficient aircraft conflict avoidance," *IEEE Transactions on Intelligent Transportation Systems*, vol. PP, no. 99, pp. 1–13, 2016.

[31] S. Sager, G. Reinelt, and H.G. Bock, "Direct Methods With Maximal Lower Bound for Mixed-Integer Optimal Control Problems," *Mathematical Programming*, vol. 118, no. 1, pp. 109–149, 2009.

[32] C. R. Hargraves and S. W. Paris, "Direct trajectory optimization using nonlinear programming and collocation," *Journal of Guidance, Control, and Dynamics*, vol. 10, no. 4, pp. 338–342, 1987.

[33] Ireland B. Walker, M. J. H. and J. Owens, "A set of modified equinoctial elements," *Celestial Mechanics*, vol. 36, pp. 409–419, July 1985.

[34] John T Betts., "Survey of numerical methods for trajectory optimization," *Journal of guidance, control, and dynamics*, vol. 21(2), pp. 193,207, 1998.

[35] Carlos R. Ortiz Longo and Steven L. Rickman, "Method for the calculation of spacecraft umbra and penumbra shadow terminator points," Technical Paper 3547, NASA, Lyndon B. Johnson Space Center, Houston, Texas, April 1995.

[36] David Morante, Manuel Sanjurjo, and Manuel Soler, "Low-thrust earth-orbit transfer optimization using analytical averaging within a sequential method," in *Advances in the Astronautical Sciences, Vail, Colorado, USA, August 8-13*, 2015.

[37] Andreas Wachter Stefan Vigerske, "*Introduction to Ipopt: A tutorial for downloading, installing and using Ipopt*," Tech. Rep., Carnegie Mellon University, April 8,2014.